nature communications

Article

https://doi.org/10.1038/s41467-025-57645-5

DeltaC and DeltaD ligands play different roles in the segmentation clock dynamics

Received: 23 July 2024

Accepted: 27 February 2025

Published online: 11 March 2025

Check for updates

Eslim Esra Alpay[1,2], Oriana Q. H. Zinani[1], Xiyan Hu[3,4], Ahmet Ay[3,5] & Ertuğrul M. Özbudak[1,2]

The vertebrate segmentation clock drives periodic somite segmentation during embryonic development. Her1 and Her7 clock proteins generate oscillatory expression of their own genes as well as that of *deltaC* in zebrafish. In turn, DeltaC and DeltaD ligands activate Notch signaling, which then activates transcription of clock genes in neighboring cells. While DeltaC and DeltaD proteins form homo- and heterodimers, only DeltaC-containing oscillatory dimers were expected to be functional. To investigate the contributions of DeltaC and DeltaD proteins on the transcription of *her1* and *her7* segmentation clock genes, we counted their transcripts by performing single molecule fluorescent in situ hybridization imaging in different genetic backgrounds of zebrafish embryos. Surprisingly, we found that DeltaD homodimers are also functional. We further found that Notch signaling promotes transcription of both *deltaC* and *deltaD* genes, thereby creating a previously unnoticed positive feedback loop. Our computational model highlighted the intriguing differential roles of DeltaC and DeltaD dimers on the clock synchronization and transcript numbers, respectively. We anticipate that a mechanistic understanding of the Notch signaling pathway will not only shed light on the mechanism driving robust somite segmentation but also inspire similar quantitative studies in other tissues and organs.

Metazoans use signaling pathways to control proper patterning of developing embryos. Notch signaling is one of those pathways, critical for both embryonic development and adult homeostasis[1]. Somites are the precursors of the vertebral disks and associated structures; sequential segmentation of somites is regulated by Notch signaling during embryonic development[2,3]. Mutations in Notch signaling pathway genes result in vertebral segmentation defects in all vertebrates (e.g., congenital scoliosis in patients)[4].

The periodic segmentation of somites from the presomitic mesoderm (PSM) is governed by the vertebrate segmentation clock. The *Hes/her* family genes constitute the core of the segmentation clock in vertebrates; their mutation results in somite segmentation defects[2,3]. Transcription of *Hes/her* family genes are activated by Notch signaling[5,6]. During somite segmentation, the Notch receptor is activated by membrane-bound Delta family ligands. Upon binding to their ligands, the intracellular domain of Notch receptors (NICD) is cleaved and transported into the nucleus and acts as a transcriptional coactivator[1]. In zebrafish, both *deltaC* and *deltaD* are also essential for somite segmentation, as mutation in either gene results in segmentation defects[7–9].

In zebrafish, the primary role of Notch signaling is to synchronize oscillations of the two segmentation clock genes, *her1* and *her7*, among neighboring cells[5,10–13]. In Notch pathway mutants, oscillations of *her1* and *her7* are initially synchronous but then gradually drift out of

[1]Division of Developmental Biology, Cincinnati Children's Hospital Medical Center, Cincinnati, OH, USA. [2]Department of Cell and Developmental Biology, Northwestern University Feinberg School of Medicine, Chicago, IL, USA. [3]Department of Mathematics, Colgate University, Hamilton, NY, USA. [4]Department of Computer Science, Colgate University, Hamilton, NY, USA. [5]Department of Biology, Colgate University, Hamilton, NY, USA.
e-mail: ozbudak@northwestern.edu

synchrony among neighboring cells[10,13]. Consequently, while earlier-forming anterior somites are intact, later-forming posterior ones are defective[7–10]. In different *delta* gene loss-of-function mutants, the strength of Notch signaling might be reduced differently, resulting in formation of varying numbers of intact somites (e.g., 3-5 in $dlc^{tw212b3}$ mutants and 7-9 in dld^{tr233} mutants)[7–9]. In zebrafish, *her1* and *her7* clock genes can still be transcribed in Notch pathway mutants, explaining why single cells can continue to display asynchronous oscillations. This is likely due to another signaling pathway (i.e., FGF) contributing to the expression of segmentation clock in Notch pathway mutants[14]. In mice, Notch signaling controls synchronized oscillations of the segmentation clock as well[15]. On the other hand, for sustained oscillations to occur, transcription rate of clock genes needs to be very strong[16]; conditions violating this requirement can result in segmentation defects[17–19].

DeltaC and DeltaD proteins form homo- and heterodimers[20]. Even though mutations in either gene result in segmentation defects, since only *deltaC* is identified as oscillating, it was hypothesized that the oscillatory DeltaC/DeltaD heterodimer is the primary ligand activating Notch signaling in zebrafish[20]. Because the onset of segmentation defects is earlier in dlc^{tw212b} mutant than dld^{tr233} mutant, it was further hypothesized that the oscillatory DeltaC/DeltaC homodimer is also functional, but the non-oscillatory DeltaD/DeltaD dimer is nonfunctional[20] (Fig. 1p). These hypotheses generate important predictions about the transcript numbers of *her1* and *her7* genes in different mutants, but these predictions have so far not been quantitatively tested. Furthermore, existing computational models of the segmentation network assume that while the transcription of *deltaC* is repressed by Her1/Her7 proteins, it is not regulated by the Notch signaling independent of Her1/Her7 proteins[16,21]. Similarly, since transcription of *deltaD* is not repressed by Her1/Her7 proteins and consequently does not oscillate, existing models also assume that Notch signaling also does not regulate transcription of *deltaD*. These critical assumptions have also been left untested.

Here, we performed quantitative single molecule fluorescent in situ hybridization (smFISH) experiments to quantify *her1* and *her7* RNAs in different mutants. Our results suggest that all above-mentioned assumptions are false: Contrary to the previous belief, the DeltaD homodimers are capable of activating Notch signaling and thereby increasing transcription of its two target segmentation clock genes, *her1* and *her7*. Moreover, Notch signaling promotes transcription of both *deltaC* and *deltaD* genes, thereby creating a hitherto unnoticed positive feedback loop.

Results

DeltaD homodimer activates transcription more than DeltaC homodimer

Individual contributions of DeltaC and DeltaD ligands on the transcription of *her1* and *her7* was previously investigated by comparing RNA levels in wild-type versus *deltaC* and/or *deltaD* mutants by both semi-quantitative FISH[5] and quantitative smFISH experiments[6]. However, three obstacles prevented an accurate one-to-one comparison and reaching a quantitative conclusion: (1) *her1* and *her7* levels oscillate synchronously in wild-type and asynchronously in mutants[13]. Thus, the dynamics of genetic backgrounds are not an "apples-to-apples" comparable. Because mutant cells oscillate asynchronously, cells at different oscillation phases will be intermingled at every spatial location. If mean expression of mutant cells at a given location is compared to that of wild-type cells at the highest oscillation phase, it will lead to one conclusion but comparing it to wild-type cells at the lowest oscillation phase will lead to the opposite conclusion. (2) Furthermore, the autoinhibitory negative feedback loop of Her1/Her7 proteins would compensate for expression level changes due to loss of NICD activity in *delta* mutants. Therefore, the comparison could be inaccurate. (3) There could be additional hidden feedback loops that would complicate interpretations due to feedback mediated compensations (see results below). To discover such hitherto hidden feedback loops and reach a definitive and quantitative conclusion, one should compare the contribution of each Delta ligand at a genetic background with comparable dynamics ("apples-to-apples" comparison) as we performed in this study.

To overcome these confounding factors, we utilized the $her1^{ci301};her7^{hu2526}$ double homozygous loss-of-function mutant as the genetic background (Fig. 1a). In this mutant, oscillations of *her1*, *her7*, and *deltaC* are arrested, the intracellular negative feedback and intercellular positive feedback loop are eliminated, preventing their compensatory effects. We used these double homozygous mutants combined with either dlc^{tw212b} and/or dld^{tr233} mutants to generate three different compound mutants: $her1^{ci301};her7^{hu2526};dlc^{tw212b}$ (Fig. 1b), $her1^{ci301};her7^{hu2526};dld^{tr233}$ (Fig. 1c) and $her1^{ci301};her7^{hu2526};dlc^{tw212b};dld^{tr233}$ (Fig. 1d). We then quantified *her1* and *her7* RNAs in these four genetic backgrounds by smFISH experiments (Fig. 1e-l).

The single cells were then pooled independently of their spatial position and plotted as a frequency graph of cells with different RNA numbers. As expected, we found that *her1* and *her7* RNAs decreased in triple and quadruple mutants as compared to those in the double mutant (Fig. 1m–o). In the $her1^{ci301};her7^{hu2526};dlc^{tw212b}$ and $her1^{ci301};her7^{hu2526};dld^{tr233}$ mutants, the only remaining functional ligand dimers would be DeltaD or DeltaC homodimers, respectively. Based on the previously proposed hypothesis[20] (Fig. 1p), one would expect *her1* and *her7* RNAs to decrease more in the $her1^{ci301};her7^{hu2526};dlc^{tw212b}$ mutant than in the $her1^{ci301};her7^{hu2526};dld^{tr233}$ mutant. Surprisingly, we obtained the opposite result, which suggests that DeltaD homodimers are also functional (Fig. 1r).

Delta proteins contribute equally to the transcription in the tailbud

Since our results suggested that the DeltaD homodimer contributes more than DeltaC homodimer to the transcription of *her1* and *her7* (when averaged across the whole PSM), we were left wondering why the onset of segmentation defects occurs earlier in dlc^{tw212b} than dld^{tr233} mutants. The segmentation clock instructs segment boundaries locally in the mid-PSM at a position called the segmental determination front[22–24]. This front is located at a distance equal to the length of three presumptive somites posterior from the last segmented somite boundary during mid-somitogenesis in zebrafish[25]. When the activity of Notch signaling is blocked, it takes approximately seven clock cycles before segmentation clock genes are desynchronized in the PSM[5,11,12]. Therefore, Notch signaling mainly operates in the tailbud to synchronize segmentation clock genes[12]. When Notch activity is blocked, only tailbud cells will spend adequate time in the PSM to become desynchronized before reaching the determination front.

Thus, we quantified how *her1* and *her7* RNAs change along the PSM in the different mutants. To that end, we averaged RNA numbers among cells located at different positions in the PSM by dividing the tissue into single-cell width sections[6,26] (Fig. 2a). We found that *her1* and *her7* RNAs decreased in the cells located at the tailbud comparably in $her1^{ci301};her7^{hu2526};dlc^{tw212b}$ and $her1^{ci301};her7^{hu2526};dld^{tr233}$ mutants (Fig. 2b-g; Group 1). These results suggest that DeltaC and DeltaD homodimers function similarly in the tailbud cells. However, because only DeltaC dimers are oscillatory, synchrony between neighboring cells will be more compromised in dlc^{tw212b} than in dld^{tr233} mutants. Consequently, even though the cumulative RNA reduction in tailbud cells is similar in both genotypes, both desynchronization of clock oscillations and the onset of segmentation defects occur earlier in dlc^{tw212b} than dld^{tr233} mutants (see computational modeling results below).

In the posterior and mid-PSM, up to the determination front, the DeltaD homodimer is more functional than the DeltaC homodimer (Fig. 2b-g; Group 2). While the segmentation clock is not relevant for

https://doi.org/10.1038/s41467-025-57645-5

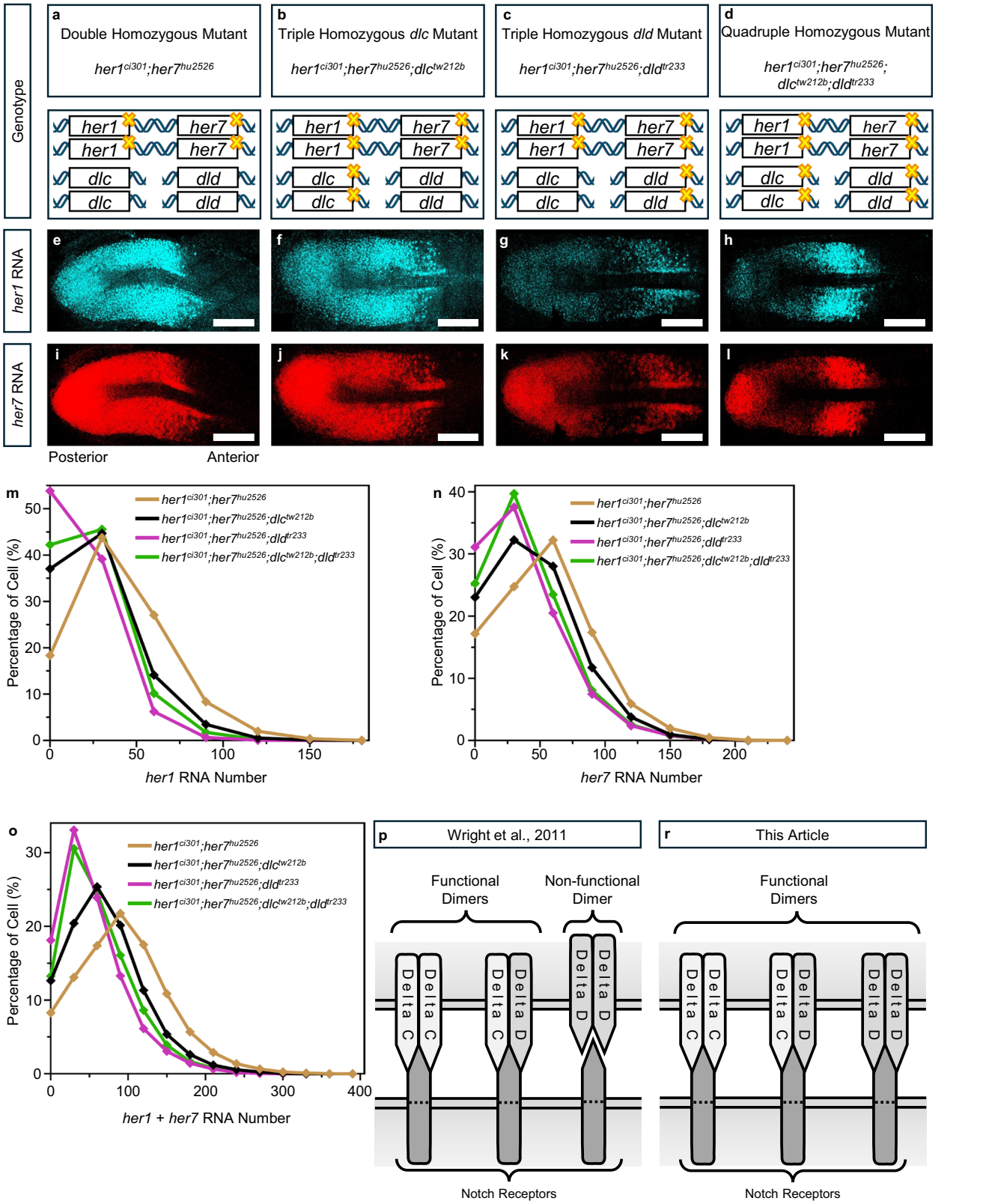

Fig. 1 | Both DeltaC and DeltaD ligands are crucial for *her* transcription. **a**–**l**, Yellow crosses indicate mutations on genes. smFISH experiment was performed in four different genotypes to show *her1* (cyan) (**e**–**h**) and *her7* (red) (**i**–**l**) RNA transcription. Representative images are maximum intensity projections of a z-stack. The scale bar is 100 µm, the left is posterior and the right is anterior end of PSM. **m**–**o**, Percentage of cells for specific *her1* (**m**), *her7* (**n**) and *her1* plus *her7* (total *her*) (**o**) RNA numbers in $her1^{ci301};her7^{hu2526}$ (dark yellow, N = 2, n = 14, c = 25030), $her1^{ci301};her7^{hu2526};dlc^{tw212b}$ (black, N = 2, n = 16, c = 28953), $her1^{ci301};her7^{hu2526};dld^{tr233}$ (purple, N = 3, n = 13, c = 23555), $her1^{ci301};her7^{hu2526};dlc^{tw212b};dld^{tr233}$ (green, N = 2, n = 11, c = 14528) genotypes. Experimental, embryo, and cell numbers are represented as N, n, and c, respectively. **p**, **r** Cartoon model for functionality of delta ligand dimers according to Wright et al[20]. (**p**), and this paper (**r**). Source data are provided as a Source Data file.

https://doi.org/10.1038/s41467-025-57645-5

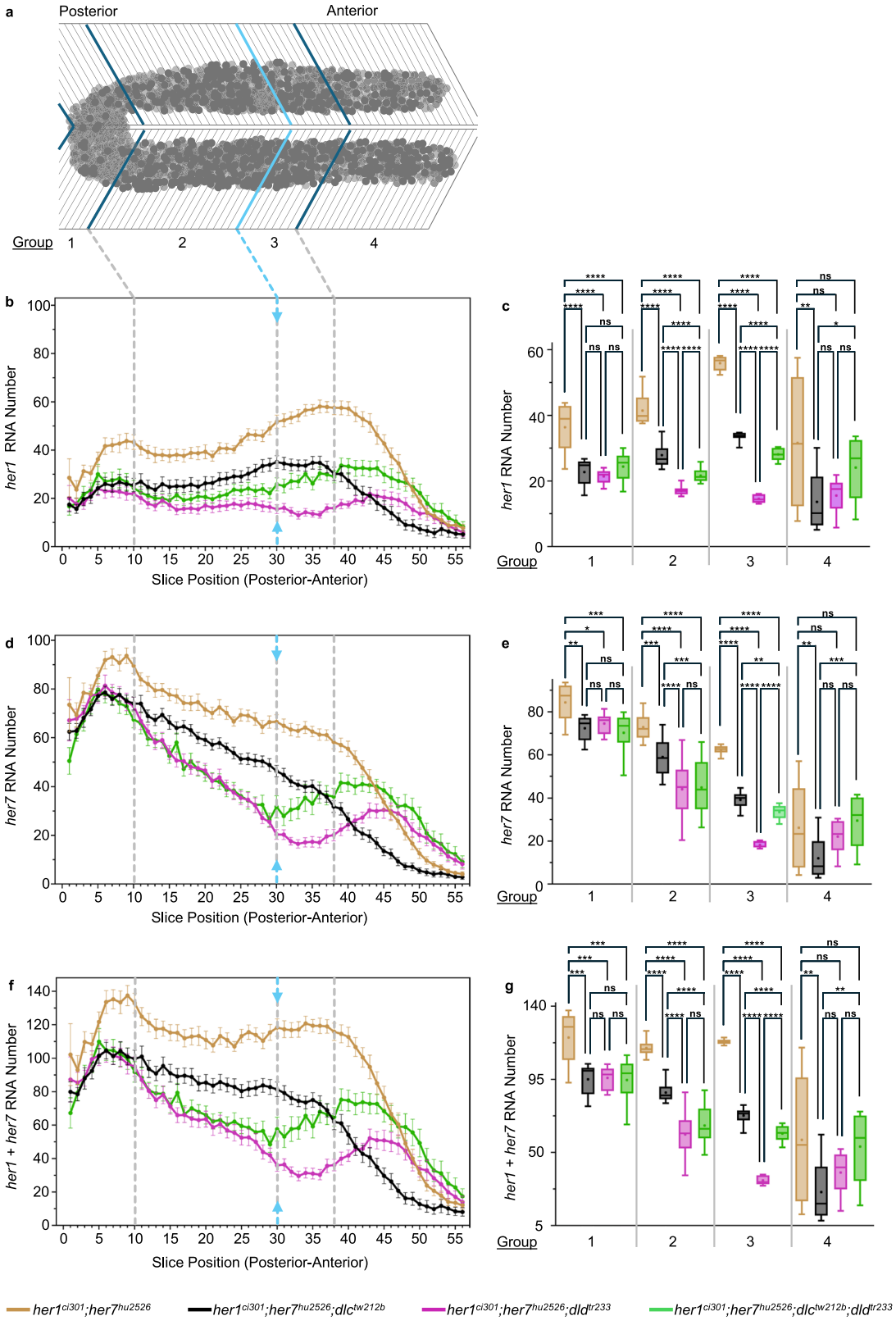

periodic boundary specification anterior to the determination front, it is critical for establishing rostrocaudal polarity of somites, which is important for later differentiation of segmented cells[22,23]. After the determination front, we observed perplexing changes in the *her1* and *her7* RNA numbers among different mutants. *her1* and *her7* RNAs started to increase in quadruple mutants as compared to first in *her1*^{ci301};*her7*^{hu2526};*dld*^{tr233} mutant (Fig. 2b–g; Group 3). In the anterior-most PSM, the *her1* and *her7* RNAs were higher in quadruple mutant than both triple mutants (Fig. 2b–g; Group 4).

While a complete explanation of this outcome awaits future studies, there are at least two non-exclusive scenarios: (1) *jagged2b* is expressed in the anterior most PSM[27]; it is possible that expression of other ligands might also be increased in *deltaC* or *deltaD* mutant backgrounds. Different ligands (e.g., Delta or Jagged) might be

Fig. 2 | *her1* and *her7* RNA counts differentially change in different parts of PSM in each mutant genotype. a The PSM tissue is divided into single-cell-wide slices and categorized into four groups. Slices ranging from 1 to 10, 11 to 30, 31 to 38, 39 to 56 are designated as groups 1, 2, 3, and 4, respectively. Group 1 covers the tailbud. Group 2 ends at the determination front (light blue line and arrows). Group 3 and 4 are separated based on changes in transcription patterns. **b** *her1* **d** *her7* and **f** *her1* plus *her7* (total *her*) RNA numbers in $her1^{ci301};her7^{hu2526}$ (dark yellow, N = 2, n = 14), $her1^{ci301};her7^{hu2526};dlc^{tw212b}$ (black, N = 2, n = 16), $her1^{ci301};her7^{hu2526};dld^{tr233}$ (purple, N = 3, n = 13), and $her1^{ci301};her7^{hu2526};dlc^{tw212b};dld^{tr233}$ (green, N = 2, n = 11) embryos are plotted from posterior to anterior direction. Experimental, and embryo numbers are represented as N, and n respectively. The average RNA number in each slice, along with 2 s.e.m., is represented by dots and error bars. Light gray dashed lines show the boundaries between four expression domains in the PSM. **c** *her1* **e** *her7* and **g** *her1* plus *her7* (total *her*) RNA numbers are compared across four genotypes, by averaging all embryos in each group, as indicated in (**a**). **c e**, **g** In Group 1, RNA numbers coming from 10 slices in $her1^{ci301};her7^{hu2526}$ (dark yellow, N = 2, n = 14, s = 234), $her1^{ci301};her7^{hu2526};dlc^{tw212b}$ (black, N = 2, n = 16, s = 288), $her1^{ci301};her7^{hu2526};dld^{tr233}$ (purple, N = 3, n = 13, s = 221), and $her1^{ci301};her7^{hu2526};dlc^{tw212b};dld^{tr233}$ (green, N = 2, n = 11, s = 181). In Group 2, RNA numbers coming from 20 slices in $her1^{ci301};her7^{hu2526}$ (dark yellow, N = 2, n = 14, s = 560), $her1^{ci301};her7^{hu2526};dlc^{tw212b}$ (black, N = 2, n = 16, s = 636), $her1^{ci301};her7^{hu2526};dld^{tr233}$ (purple, N = 3, n = 13, s = 514), and $her1^{ci301};her7^{hu2526};dlc^{tw212b};dld^{tr233}$ (green, N = 2, n = 11, s = 420). In Group 3, RNA numbers coming from 8 slices in $her1^{ci301};her7^{hu2526}$ (dark yellow, N = 2, n = 14, s = 224), $her1^{ci301};her7^{hu2526};dlc^{tw212b}$ (black, N = 2, n = 16, s = 256), $her1^{ci301};her7^{hu2526};dld^{tr233}$ (purple, N = 3, n = 13, s = 206), and $her1^{ci301};her7^{hu2526};dlc^{tw212b};dld^{tr233}$ (green, N = 2, n = 11, s = 172). In Group 4, RNA numbers coming from 18 slices in $her1^{ci301};her7^{hu2526}$ (dark yellow, N = 2, n = 14, s = 494), $her1^{ci301};her7^{hu2526};dlc^{tw212b}$ (black, N = 2, n = 16, s = 519), $her1^{ci301};her7^{hu2526};dld^{tr233}$ (purple, N = 3, n = 13, s = 442), and $her1^{ci301};her7^{hu2526};dlc^{tw212b};dld^{tr233}$ (green, N = 2, n = 11, s = 366). Experimental, embryo, and slice data numbers are represented as N, n, and s, respectively. Significance test is performed in each group separately. The levels of significance are *p < 0.05, **p < 0.01, ***p < 0.001, ****p < 0.0001. Exact p-values of the significance tests are put into Supplementary Table 3. The whisker plots show the median (line), quartiles (box), mean (plus sign), as well as the minimum and maximum (whiskers). Source data are provided as a Source Data file.

competing in binding to Notch receptors in the anterior PSM. If other ligands activate Notch signaling more than DeltaC and DeltaD, they would be relieved from that competition when both *deltaC* and *deltaD* are mutated. (2) Alternatively, potential post-translation changes of the Delta ligands might convert some of the dimers from trans-activator to cis-inhibitor (or dual-functional) in the anterior PSM. Correspondingly, one of the proteins known to regulate Delta function, Lunatic fringe, is expressed in the anterior but not in the posterior and mid-PSM in zebrafish[28]. Lunatic fringe can modify Notch signaling dynamics in the chick and mouse PSM[15,29–31]. Future studies are needed to identify the contributions of different mechanisms modifying the impact of Notch signaling on the transcription of *her1* and *her7* in the anterior PSM.

DeltaC and DeltaD are the primary ligands activating transcription

Notch signaling can be activated by several ligands, but only *dlc* and *dld* mutants result in segmentation defects in zebrafish[32]. We tested whether pharmacological inhibition of gamma-secretase (γ-Secretase) activity (i.e., blocking cleavage of NICD) in quadruple mutants can affect *her1* and *her7* RNA numbers (Fig. 3a). To that end, we treated quadruple mutants with Compound E to block γ-Secretase activity starting from mid-gastrulation stages and quantified *her1* and *her7* RNAs in mid-somitogenesis stages (Fig. 3b–e). Average RNA numbers did not change significantly when the data from all the single cells were pooled together irrespective of their positions (Fig. 3f–h). When we plotted the data based on cell positional information, we found that average *her1* and *her7* RNAs did not change in cells located in the tailbud, posterior PSM, and mid-PSM (Fig. 3i–n; Groups 1-3).

In the anterior-most PSM, *her1* and *her7* RNAs slightly decreased in Compound-E treated mutants as compared to controls, albeit not passing the significance test for all comparisons (Fig. 3i–n; Group 4). Interestingly, *her1* and *her7* RNAs in this region are higher in quadruple mutants compared to triple mutants (Fig. 2c–g). Overall, both outcomes could be due to several non-exclusive scenarios as discussed in the preceding section above.

Transcription of *her1* and *her7*, although decreased, still occur in the quadruple mutants (even when γ-Secretase activity is blocked). This is because Notch signaling is only one of the transcriptional regulators of *her1* and *her7*. Several other transcription factors are regionally expressed in the tissue[2,32]. Their contributions on transcription of *her1* and *her7* at different spatial locations will be investigated in future studies.

Notch signaling promotes transcription of *deltaC* and *deltaD*

Oscillatory Her1 and Her7 proteins repress transcription of *deltaC* and thereby drive its oscillations. In previously proposed regulatory networks and computational models, Notch signaling is assumed not to affect transcription of *deltaC* in zebrafish[12,16,21,33]. Because *deltaD* is not repressed by Her1 and Her7 proteins, its expression does not oscillate in zebrafish. Therefore, Notch signaling is also assumed not to affect transcription of *deltaD*. It is difficult to test these assumptions by comparing *deltaC* and *deltaD* transcript counts between wild-type and single mutants due to several obstacles described in the preceding sections. In addition to those obstacles, there is one additional one: For example, if Notch signaling promotes transcription of *deltaC*, *deltaC* level is expected to be decreased in Notch pathway mutants due to loss of activation. But Notch signaling also activates transcription of *her1* and *her7*; their levels will also decrease in Notch pathway mutants, and consequently, reduction in Her1 and Her7 proteins will derepress *deltaC*. This derepression will counteract loss of activation, resulting in misleading conclusions.

To overcome these obstacles, we again utilized the same genetic backgrounds in which the several feedback loops and differences in dynamical states are eliminated. We performed smFISH experiments to compare *deltaC* and *deltaD* RNAs between $her1^{ci301};her7^{hu2526}$ and $her1^{ci301};her7^{hu2526};dlc^{tw212b};dld^{tr233}$ mutants (Figs. 4a, b and 5a, b). Contrary to the previous assumptions, we found that both *deltaC* and *deltaD* RNAs decreased in quadruple mutants as compared to $her1^{ci301};her7^{hu2526}$ mutants (Figs. 4c–e and 5c–e). The spatial profile of *deltaC* RNA revealed that while its transcription is reduced in quadruple mutants as compared to $her1^{ci301};her7^{hu2526}$ mutants in most of the posterior and mid-PSM, an opposite effect is observed in the anterior PSM (Fig. 4d, e). The latter outcome might be due to the same hidden mechanism modifying the impact of Notch signaling on transcription of three oscillatory genes (*her1*, *her7*, and *deltaC*) in the anterior PSM, as discussed above (Fig. 2c–g). Overall, this result unearths a hitherto unnoticed positive feedback loop in the segmentation regulatory network.

We realized a potential caveat in our quantification of *deltaD* RNA: the dld^{tr233} mutation, but not the dlc^{tw212b} mutation, creates a premature termination codon (PTC) in the *dld* gene. PTCs can sometimes lead to nonsense mediated decay of their transcripts. Therefore, the reduction in *deltaD* RNA in quadruple mutant as compared to double mutant could in part be due to nonsense mediated decay.

To reassess the potential role of Notch signaling on *deltaD* transcription, we decided to inhibit Notch signaling also pharmaceutically. Hence, we treated $her1^{ci301};her7^{hu2526}$ double mutants with Compound E or DMSO (control) (Fig. 5f, g). We again found that *deltaD* RNAs decreased when γ-Secretase activity is inhibited (Fig. 5h). The reduction in *deltaD* RNAs is lower when Notch signaling is pharmaceutically inhibited as compared to the genetic inhibition (Fig. 5c–e, h–j). This difference could be due to either incomplete inhibition of Notch signaling by Compound E and/or nonsense mediated decay of *deltaD*

https://doi.org/10.1038/s41467-025-57645-5

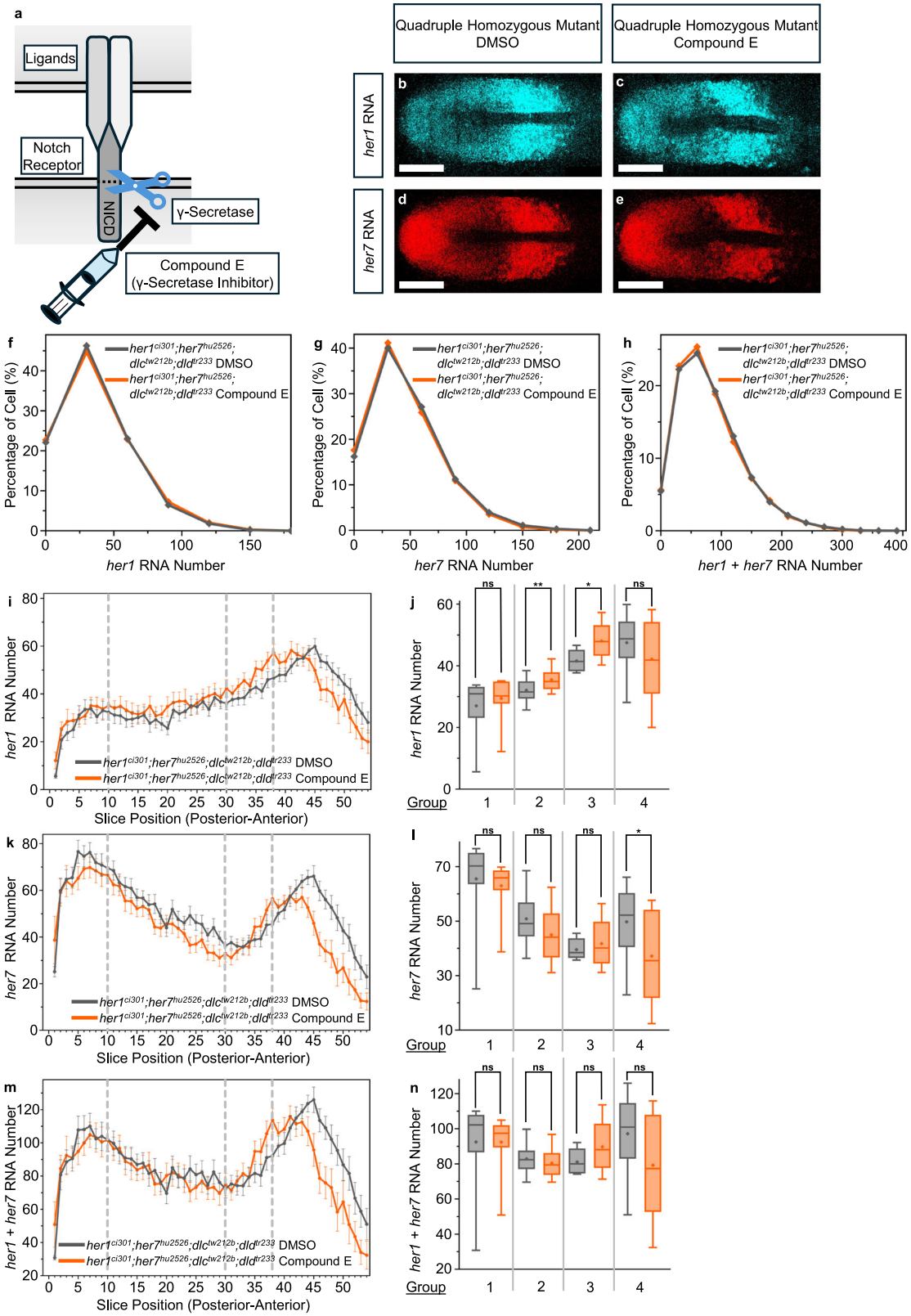

RNA with *dld*^{tr233} mutation. Nonetheless, these results showed that Notch signaling promotes transcription of both of its two ligands in the zebrafish PSM (Fig. 5k)

We currently do not know whether NICD directly or indirectly activates transcription of *deltaC* and *deltaD*. Currently, the regulatory regions driving transcription of *deltaC* and *deltaD* in the zebrafish PSM are unknown. Nonetheless, bioinformatics analysis found several putative SuH/RBPJK binding sites within 20 kb region flanking both genes (10 kb upstream of transcription start site and 10 kb downstream of transcription end, including the transcribed regions) (Table S1). Future research will investigate whether NICD directly activates transcription of either ligand gene via some of these regulatory sites.

Fig. 3 | DeltaC and DeltaD mediate most of the Notch activity in the PSM. **a** Cartoon model showing how Compound E is blocking NICD cleavage by inhibiting gamma secretase (γ-Secretase) activity. Syringe symbol represents the application of Compound E drug, while the scissor symbol represents the γ-Secretase activity. **b**–**e** Transcription of *her1* (cyan) (**b**, **c**) and *her7* (red) (**d**, **e**) RNA in DMSO and Compound E treated *her1*^{ci301};*her7*^{hu2526};*dlc*^{tw212b};*dld*^{tr233} embryos. Representative images are maximum intensity projections of a z-stack. The scale bar is 100 µm. **f**–**h** Histograms showing the percentage of cells with different *her1* (**f**), *her7* (**g**) and *her1* plus *her7* (total *her*) (**h**) RNA numbers in DMSO (gray, N = 2, n = 9, c = 14,000), and Compound E (orange, N = 2, n = 8, c = 9107) treated *her1*^{ci301};*her7*^{hu2526};*dlc*^{tw212b};*dld*^{tr233} embryos. Experimental, embryo, and cell numbers are represented as N, n, and c, respectively. **i** *her1* **k** *her7* and **m** *her1* plus *her7* (total *her*) RNA numbers are plotted throughout the PSM (posterior to anterior) in *her1*^{ci301};*her7*^{hu2526};*dlc*^{tw212b};*dld*^{tr233} embryos treated with DMSO (gray, N = 2, n = 9), and Compound E (orange, N = 2, n = 8). The average RNA number in each slice, along with 2 s.e.m., is represented by dots and error bars. **j** *her1* **l** *her,7* and **n** *her1* plus *her7* (total *her*) RNA numbers are compared in DMSO and Compound E treated embryos, by averaging all embryos in each group, as indicated in Fig. 2a. **j**, **l**, **n** In Group 1, RNA numbers coming from 10 slices in *her1*^{ci301};*her7*^{hu2526};*dlc*^{tw212b};*dld*^{tr233} embryos treated with DMSO (gray, N = 2, n = 9, s = 150), and Compound E (orange, N = 2, n = 8, s = 119). In Group 2, RNA numbers coming from 20 slices in *her1*^{ci301};*her7*^{hu2526};*dlc*^{tw212b};*dld*^{tr233} embryos treated with DMSO (gray, N = 2, n = 9, s = 355), and Compound E (orange, N = 2, n = 8, s = 308). In Group 3, RNA numbers coming from 8 slices in *her1*^{ci301};*her7*^{hu2526};*dlc*^{tw212b};*dld*^{tr233} embryos treated with DMSO (gray, N = 2, n = 9, s = 144), and Compound E (orange, N = 2, n = 8, s = 127). In Group 4, RNA numbers coming from 16 slices in *her1*^{ci301};*her7*^{hu2526};*dlc*^{tw212b};*dld*^{tr233} embryos treated with DMSO (gray, N = 2, n = 9, s = 288), and Compound E (orange, N = 2, n = 8, s = 253). Experimental, embryo, and slice data numbers are represented as N, n, and s, respectively. Significance test is performed in each group separately. The levels of significance are *p < 0.05, **p < 0.01, ***p < 0.001, ****p < 0.0001. Exact p-values of the significance tests are put into Supplementary Table 3. The whisker plots show the median (line), quartiles (box), mean (plus sign), as well as the minimum and maximum (whiskers). Source data are provided as a Source Data file.

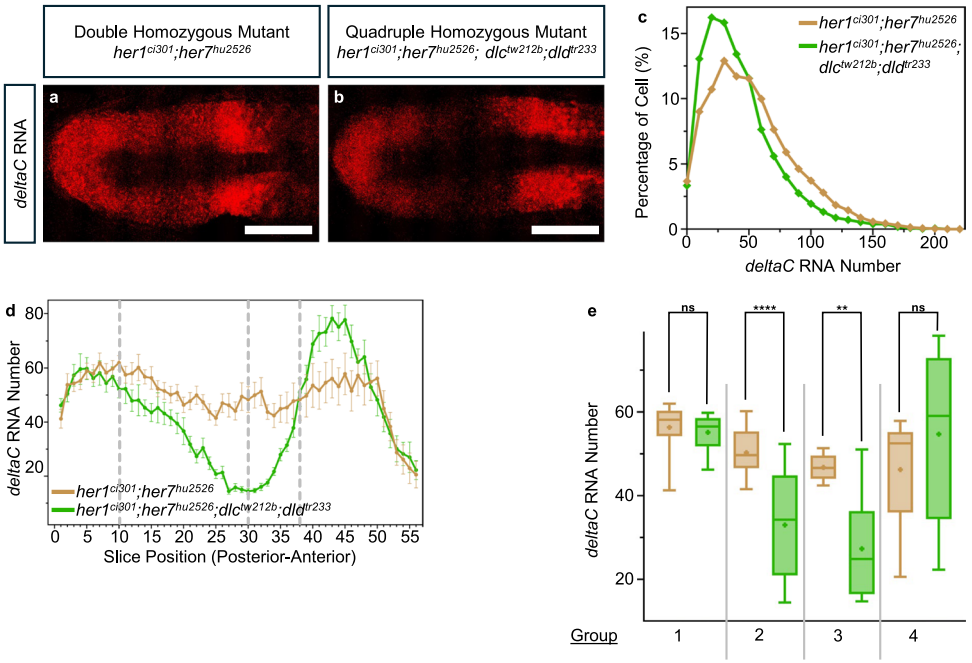

Fig. 4 | Notch signaling promotes *deltaC* transcription. **a**, **b** Transcription of *deltaC* (red) RNA in *her1*^{ci301};*her7*^{hu2526} and *her1*^{ci301};*her7*^{hu2526};*dlc*^{tw212b};*dld*^{tr233} embryos. Representative images are maximum intensity projections of a z-stack. The scale bar is 100 µm. **c** *deltaC* RNA number per cell in *her1*^{ci301};*her7*^{hu2526} (dark yellow, N = 1, n = 7, c = 16259), and *her1*^{ci301};*her7*^{hu2526};*dlc*^{tw212b};*dld*^{tr233} (green, N = 1, n = 5, c = 7386) embryos. The levels of significance are *p < 0.05, **p < 0.01, ***p < 0.001, ****p < 0.0001. Experimental, embryo, and cell numbers are represented as N, n, and c, respectively. **d** *deltaC* RNA number is plotted throughout the PSM (posterior to anterior) in *her1*^{ci301};*her7*^{hu2526} (dark yellow, N = 1, n = 7), and *her1*^{ci301};*her7*^{hu2526};*dlc*^{tw212b};*dld*^{tr233} (green, N = 1, n = 5) embryos. The average mRNA number in each slice represented as dots, mean data, and 2 s.e.m are used in the graph. **e** Comparison of the *deltaC* RNA number across two genotypes, by averaging all embryos in each group, as indicated in Fig. 2a. In Group 1, RNA numbers coming from 10 slices in *her1*^{ci301};*her7*^{hu2526} (dark yellow, N = 1, n = 7, s = 134), and *her1*^{ci301};*her7*^{hu2526};*dlc*^{tw212b};*dld*^{tr233} (green, N = 1, n = 5, s = 98). In Group 2, RNA numbers coming from 20 slices in *her1*^{ci301};*her7*^{hu2526} (dark yellow, N = 1, n = 7, s = 279), and *her1*^{ci301};*her7*^{hu2526};*dlc*^{tw212b};*dld*^{tr233} (green, N = 1, n = 5, s = 200). In Group 3, RNA numbers coming from 8 slices in *her1*^{ci301};*her7*^{hu2526} (dark yellow, N = 1, n = 7, s = 112), and *her1*^{ci301};*her7*^{hu2526};*dlc*^{tw212b};*dld*^{tr233} (green, N = 1, n = 5, s = 80). In Group 4, RNA numbers coming from 18 slices in *her1*^{ci301};*her7*^{hu2526} (dark yellow, N = 1, n = 7, s = 234), and *her1*^{ci301};*her7*^{hu2526};*dlc*^{tw212b};*dld*^{tr233} (green, N = 1, n = 5, s = 177). Experimental, embryo, and slice data numbers are represented as N, n, and s, respectively. Significance test is performed in each group separately. The levels of significance are *p < 0.05, **p < 0.01, ***p < 0.001, ****p < 0.0001. Exact p-values of the significance tests are put into Supplementary Table 3. The whisker plots show the median (line), quartiles (box), mean (plus sign), as well as the minimum and maximum (whiskers). Source data are provided as a Source Data file.

Computational modeling highlights differential effects of DeltaC and DeltaD dimers

As discussed above, single *dlc*^{tw212b} mutant gives an earlier and stronger phenotype than that of single *dld*^{tr233} mutant. Yet, surprisingly, DeltaD dimer increases *her1* and *her7* RNAs more than DeltaC dimer does. To bring insight into these two contradictory outcomes, we updated our previously developed mathematical model[21,33] of the zebrafish segmentation clock network based on current experimental findings: (1) Delta dimers are now explicitly introduced and differentiated from each other in the equations. (2) The identified intercellular positive feedback loops are added to the regulatory network. Computational simulations are performed only in two neighboring cells to reduce the computational burden, and reaction parameters are searched in physiological ranges as before[21,33].

We found several parameter sets satisfying these four experimentally-derived constraints: (1) *dlc*^{tw212b} mutants will cause earlier onset of desynchronization (i.e., reflecting the phenotype in simulations) than single *dld*^{tr233} mutants (Fig. 6a–d). (2) double

https://doi.org/10.1038/s41467-025-57645-5

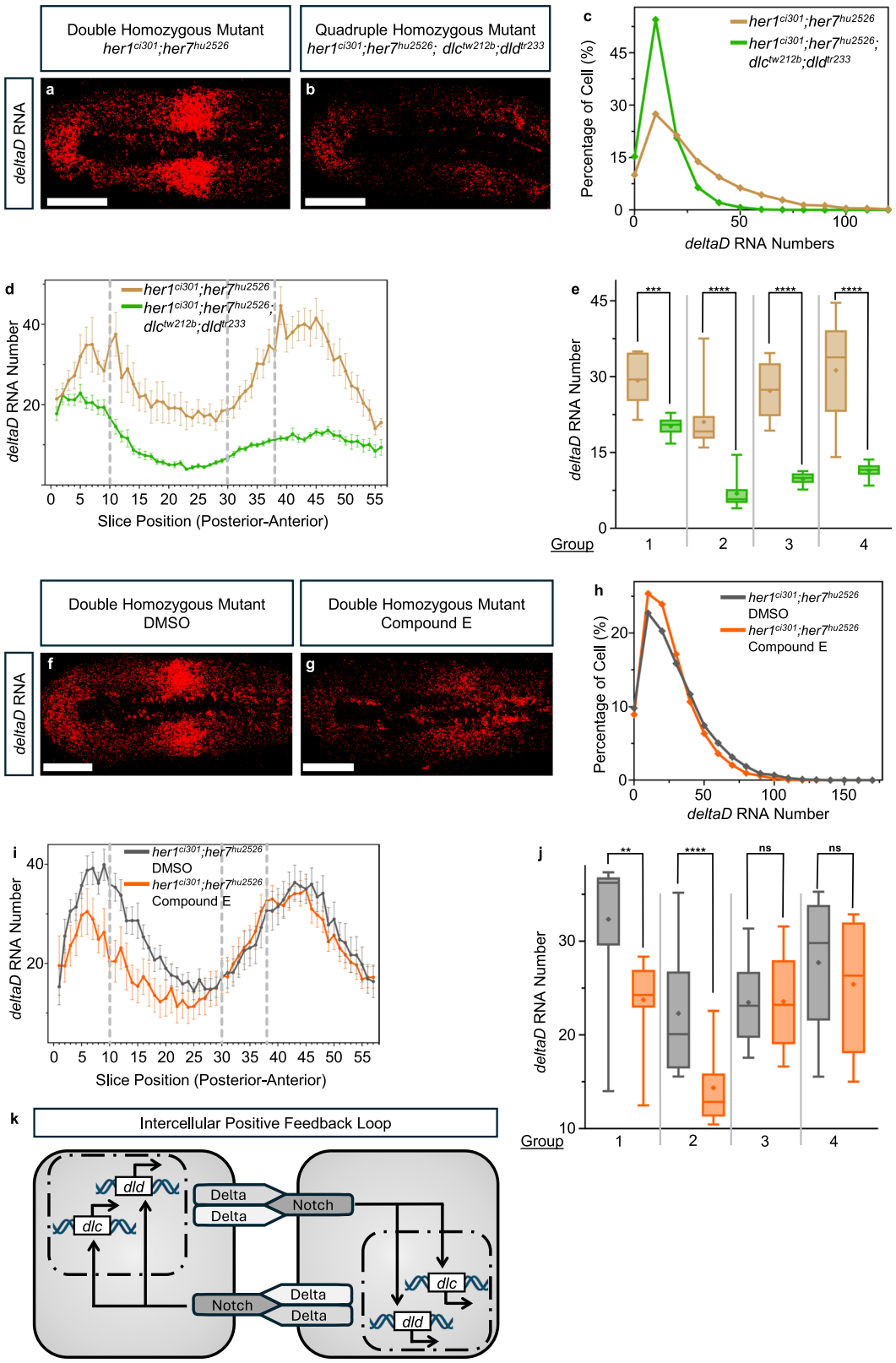

$dlc^{tw212b};dld^{tr233}$ mutant phenotype will be similar to that of single dlc^{tw212b} mutant[8] (Fig. 6a–d). (3) *her1* and *her7* RNA numbers will be reduced more in $her1^{ci301};her7^{hu2526};dld^{tr233}$ mutants than in $her1^{ci301};her7^{hu2526};dlc^{tw212b}$ mutants (Fig. 6e). (4) *her1* and *her7* RNA numbers will be similar in $her1^{ci301};her7^{hu2526};dld^{tr233}$ and $her1^{ci301};her7^{hu2526};dlc^{tw212b};dld^{tr233}$ mutants (Fig. 6e). Overall, the simulations provided insight into why dlc^{tw212b} mutant shows a stronger phenotype than dld^{tr233} mutant while segmentation clock transcripts are reduced more in dld^{tr233} mutant than in dlc^{tw212b} mutant.

We next assessed the potential benefit of the identified positive feedback loops in the somite segmentation network. A previous computational model argued that while negative feedback loops are necessary and sufficient for generating oscillations, an additional positive feedback loop can make the oscillations more robust[34]. Thus,

Fig. 5 | Notch signaling promotes *deltaD* transcription. a, **b** Transcription of *deltaD* (red) RNA in *her1*^{ci301};*her7*^{hu2526} and *her1*^{ci301};*her7*^{hu2526}; *dlc*^{tw212b};*dld*^{tr233} embryos. Representative images are single section of a z-stack. The scale bar is 100 µm. **c** *deltaD* RNA number per cell in *her1*^{ci301};*her7*^{hu2526} (dark yellow, N = 1, n = 7, c = 8959), and *her1*^{ci301};*her7*^{hu2526};*dlc*^{tw212b};*dld*^{tr233} (green, N = 1, n = 10, c = 12313) embryos. Experimental, embryo, and cell numbers are represented as N, n, and c, respectively. **d** *deltaD* RNA number is plotted throughout the PSM (posterior to anterior) in *her1*^{ci301};*her7*^{hu2526} (dark yellow, N = 1, n = 7), and *her1*^{ci301};*her7*^{hu2526};*dlc*^{tw212b};*dld*^{tr233} (green, N = 1, n = 10) embryos. The average RNA number in each slice represented as dots, mean data, and 2 s.e.m are used in the graph. **e** Comparison of the *deltaD* RNA number across two genotypes, by averaging all embryos in each group, as indicated in Fig. 2a. In Group 1, RNA numbers coming from 10 slices in *her1*^{ci301};*her7*^{hu2526} (dark yellow, N = 1, n = 7, s = 102), and *her1*^{ci301};*her7*^{hu2526};*dlc*^{tw212b};*dld*^{tr233} (green, N = 1, n = 10, s = 182). In Group 2, RNA numbers coming from 20 slices in *her1*^{ci301};*her7*^{hu2526} (dark yellow, N = 1, n = 7, s = 254), and *her1*^{ci301};*her7*^{hu2526};*dlc*^{tw212b};*dld*^{tr233} (green, N = 1, n = 10, s = 387). In Group 3, RNA numbers coming from 8 slices in *her1*^{ci301};*her7*^{hu2526} (dark yellow, N = 1, n = 7, s = 110), and *her1*^{ci301};*her7*^{hu2526};*dlc*^{tw212b};*dld*^{tr233} (green, N = 1, n = 10, s = 160). In Group 4, RNA numbers coming from 18 slices in *her1*^{ci301};*her7*^{hu2526} (dark yellow, N = 1, n = 7, s = 241), and *her1*^{ci301};*her7*^{hu2526};*dlc*^{tw212b};*dld*^{tr233} (green, N = 1, n = 10, s = 303). Experimental, embryo, and slice data numbers are represented as N, n, and s, respectively. Significance test is performed in each group separately. The levels of significance are *p < 0.05, **p < 0.01, ***p < 0.001, ****p < 0.0001. Exact p-values of the significance tests are put into Supplementary Table 3. The whisker plots show the median (line), quartiles (box), mean (plus sign), as well as the minimum and maximum (whiskers). **f**, **g** Transcription of *deltaD* (red) RNA in DMSO and Compound E treated *her1*^{ci301};*her7*^{hu2526} embryos. Representative images are single section of a z-stack. The scale bar is 100 µm. **h** Histogram showing the percentage of cells with different numbers of *deltaD* RNA in DMSO (gray, N = 1, n = 12, c = 27947), and Compound E (orange, N = 1, n = 10, c = 23007) treated *her1*^{ci301};*her7*^{hu2526} embryos. Experimental, embryo, and cell numbers are represented as N, n and c, respectively. **i** *deltaD* RNA number is plotted throughout the PSM (posterior to anterior) in DMSO (gray, N = 1, n = 12), and Compound E (orange, N = 1, n = 10) treated *her1*^{ci301};*her7*^{hu2526} embryos. The average RNA number in each slice represented as dots, mean data, and 2 s.e.m are used in the graph. **j**, Comparison of the *deltaD* RNA number between two conditions, by averaging all embryos in each group, as indicated in Fig. 2a. In Group 1, RNA numbers coming from 10 slices in *her1*^{ci301};*her7*^{hu2526} embryos treated with DMSO (gray, N = 1, n = 12, s = 220), and Compound E (orange, N = 1, n = 10, s = 186). In Group 2, RNA numbers coming from 20 slices in *her1*^{ci301};*her7*^{hu2526} embryos treated with DMSO (gray, N = 1, n = 12, s = 480), and Compound E (orange, N = 1, n = 10, s = 400). In Group 3, RNA numbers coming from 8 slices in *her1*^{ci301};*her7*^{hu2526} embryos treated with DMSO (gray, N = 1, n = 12, s = 192), and Compound E (orange, N = 1, n = 10, s = 160). In Group 4, RNA numbers coming from 18 slices in *her1*^{ci301};*her7*^{hu2526} embryos treated with DMSO (gray, N = 1, n = 12, s = 429), and Compound E (orange, N = 1, n = 10, s = 360). Experimental, embryo, and slice data numbers are represented as N, n, and s, respectively. Significance test is performed in each group separately. The levels of significance are *p < 0.05, **p < 0.01, ***p < 0.001, ****p < 0.0001. Exact p-values of the significance tests are put into Supplementary Table 3. The whisker plots show the median (line), quartiles (box), mean (plus sign), as well as the minimum and maximum (whiskers). **k** Cartoon model showing the currently identified intercellular positive feedback loop for both *deltaC* and *deltaD*. Source data are provided as a Source Data file.

we simulated the wild-type segmentation network with or without the positive feedback loops. We found that the positive feedback loops increase the amplitude of *deltaC* oscillations and consequently increase the synchronization of the segmentation clock oscillations between neighboring cells (Fig. 6f–i).

Discussion

Notch signaling plays a critical role in somite segmentation in vertebrates[2]. In humans, mutations in the pathway genes result in vertebral segmentation defects[4]. In zebrafish, mutations in two *delta* genes eventually result in failure of segmentation, save for the anterior-most somites. The primary function of Notch signaling is to synchronize segmentation clock oscillations among neighboring cells[5,10–13]. Delta ligands form both homo- and heterodimers[20]. However, because expression of only *deltaC* oscillates, it was thought that only DeltaC-containing dimers contribute to the transcription of segmentation clock genes in zebrafish[20]. Furthermore, because *deltaC* is repressed by the segmentation clock proteins[24], it was thought that transcription of *deltaC* is exclusively regulated by them but not by the Notch signaling. Because expression of *deltaD* is not oscillatory (due to lack of repression), it was also assumed not to be regulated by Notch signaling. Testing these assumptions would have been difficult by comparing wild-type and single *delta* gene mutants and by performing non-quantitative experiments.

In this study, we utilized the non-oscillatory double *her1*^{ci301};*her7*^{hu2526} mutant as a genetic background to eliminate compensatory feedback loops and oscillations. We then performed quantitative smFISH experiments to count transcripts of three oscillating genes in single cells in intact PSM tissues. Our results argued against previous assumptions in the field. We found that numbers of *her1* and *her7* RNAs decreased more in *her1*^{ci301};*her7*^{hu2526};*dld*^{tr233} mutants than in *her1*^{ci301};*her7*^{hu2526};*dlc*^{tw212b} mutants, suggesting that DeltaD homodimers are functional as well. We also found that transcription of both *deltaC* and *deltaD* are promoted by Notch signaling, unearthing a previously missed intercellular feedback loop in the zebrafish segmentation network. An updated computational model successfully recapitulated several experimental observations highlighting the differential impacts of DeltaC and DeltaD ligands on synchronization and transcript numbers of the segmentation clock. Our computational model also showed that the identified positive feedback loops could enhance the synchrony of oscillations between neighboring cells.

Interestingly, Notch1 protein level was shown to oscillate in a Notch signaling dependent manner both in chick and mouse, creating an intracellular feedback loop[35]. While the wiring of the feedback (inter- or intracellular) and molecules involved (Delta or Notch) differ among species, our results highlight conservation of a second positive feedback loop in the system. Future studies are needed to discern the advantages of the coupled feedback loops conferring to the segmentation clock network in each species.

We anticipate our results will promote the development of more accurate computation models in the field. Likewise, future experimental efforts might similarly reveal additional roles for different ligand pairs in other tissues during embryonic development and adult homeostasis.

Methods

Fish stocks

her1^{ci302};*her7*^{hu2526} (loss-of-function mutation) double mutant[19] was used as the non-oscillating background. *dlc*$^{tw212b/tw212b}$[8] and *dld*$^{tr233/tr233}$[9] were mated with *her1*^{ci302};*her7*^{hu2526} mutant to generate *her1*^{ci302};*her7*^{hu2526};*dlc*^{tw212b}, *her1*^{ci302};*her7*^{hu2526};*dld*^{tr233} and *her1*^{ci302};*her7*^{hu2526};*dlc*^{tw212b};*dld*^{tr233}. AB wild-type fish line was used to test the effectiveness of Compound E drug. All the fish experiments were performed under the ethical guidelines of Cincinnati Children's Hospital Medical Center and Northwestern University Feinberg School of Medicine with the approved animal protocols: Protocol # 2020-0031 and Protocol # IS00028088, respectively. Sex is not determined chromosomally and is fixed several weeks after fertilization in zebrafish. We used embryos less than one day post fertilization. Thus, we could not perform sex-based analysis. Because embryos used in this study are expected to be approximately of equal number of each sex, we do not discriminate against a particular sex in our studies.

Pharmacological treatments

Compound E (γ-secretase inhibitor XXI) (Millipore Sigma, CAS# 209986-17-4) was used to inhibit Notch signaling. A concentration of 50 µM Compound E was sufficient to observe the drug effect, indicated by a broken boundary in wild-type embryos (Supplementary Fig. 1). As

https://doi.org/10.1038/s41467-025-57645-5

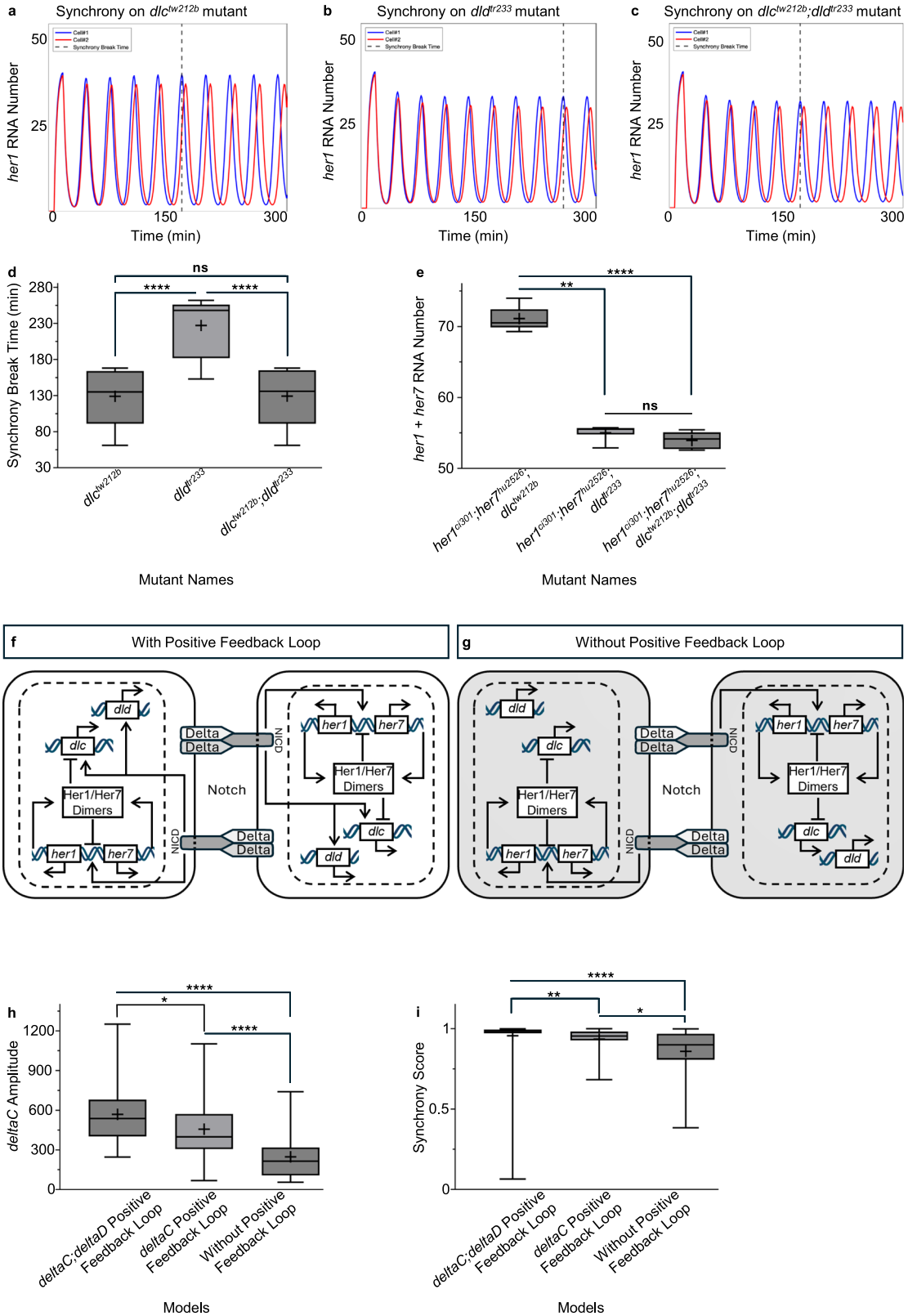

a control, DMSO was used in each experiment. Wild-type, *her1*^{ci302};*her7*^{hu2526}, and *her1*^{ci302};*her7*^{hu2526};*dlc*^{tw212b};*dld*^{tr233} embryos were raised at 28 °C until 50–75% epiboly stage, dechorionated, and treated with either Compound E (at a final concentration of 50 μM) or DMSO. The embryos were raised at 23 °C until they reached 12-14 somite stage and fixed with 4% PFA at room temperature.

smFISH experiments and Imaging

smFISH experiments and confocal imaging were conducted[36] with the following changes. Membrane-localized GFP was injected into one-cell-stage mutant embryos. The embryos were collected from at least 4 pairs of fish breedings, raised at 23 °C until they reached 12-14 somite stage, and fixed with 4% PFA at room temperature. Since the mutant

Fig. 6 | Computational modeling recapitulated each Delta ligand impacting different dynamics of the segmentation clock. a–c Representative simulations illustrating the synchronization between two cells in the model for single *dlc*^{tw212b} (**a**) single *dld*^{tr233} (**b**) and double *dlc*^{tw212b};*dld*^{tr233} mutants (**c**). **d**, **e** The whisker plots representing the average for the measures indicated. Average synchronization break time (determined when the synchronization score fall below a threshold of 0.8) in *dlc*^{tw212b}, *dld*^{tr233}, and *dlc*^{tw212b};*dld*^{tr233} mutants (**d**). Average *her1* plus *her7* RNA numbers in *her1*^{ci301};*her7*^{hu2526};*dlc*^{tw212b}, *her1*^{ci301};*her7*^{hu2526};*dld*^{tr233} and *her1*^{ci301};*her7*^{hu2526};*dlc*^{tw212b};*dld*^{tr233} mutants (**e**). **f**, **g** Cartoon showing the network with (**f**) or without (**g**) the positive feedback loop. **h**, **i** The whisker plots showing the amplitude (**h**), and synchrony score (the Pearson correlation over consecutive peak-to-trough phases) (**i**) in wild-type embryos. The whisker plots show the median (line), quartiles (box), mean (plus sign), as well as the minimum and maximum (whiskers). Significance test is performed in each plot separately. The levels of significance are *p < 0.05, **p < 0.01, ***p < 0.001, ****p < 0.0001. Exact p-values of the significance tests are put into Supplementary Table 3. Network conditions are positive feedback loop on both *deltaC* and *deltaD*, positive feedback loop only on *deltaC*, and no positive feedback loop. Source data are provided as a Source Data file.

embryos do not have intact somite boundaries, 12-14 somite stages are identified according to their tail and yolk shape (Supplementary Fig. 2). The smFISH experiment was performed with Dr-*her1*-LE2-C3 (Cat# 433201-C3) and Dr-*her7*-C1 (Cat# 428611) to detect *her1* and *her7* RNAs in four different mutant embryos. Dr-*dlc*-C2 (Cat# 559331-C2) was used to detect *deltaC* RNA number in *her1*^{ci302};*her7*^{hu2526} and *her1*^{ci302};*her7*^{hu2526};*dlc*^{tw212b};*dld*^{tr233} mutants. Dr-*dld*-C2 (Cat# 1133731-C2) was used to detect *deltaD* RNA in *her1*^{ci302};*her7*^{hu2526} and *her1*^{ci302};*her7*^{hu2526};*dlc*^{tw212b};*dld*^{tr233} mutants. Amp4 B was used when labeling *her1* and *her7* transcripts, and Amp4 A was used when labeling *deltaC* and *deltaD* transcripts. For amplifying membrane labels, immunohistochemistry (IHC) was performed after the smFISH experiment. Anti-GFP Chicken polyclonal antibody (either Invitrogen, Cat# A10262 (Lot# 2321831) or Abcam, Cat# ab13970, both at 1:200 dilution) was used as the primary antibody and Alexa Fluor 488 goat anti-chicken IgY H + L (Invitrogen, Cat# A11039 (Lot# 2420700), at 1:200 dilution) was used as the secondary antibody. Hoechst trihydrochloride (H3570, Invitrogen) was used to stain nuclei at the concentration of 7.5 mg/mL. Samples were mounted with ProLong Gold Antifade Reagent (Life Technologies, Cat# P36934), and imaged by using Nikon A1R HD confocal on a TiE microscope with an Apo TIRF 100x Oil DIC N2 objective and resonant scanner. To image whole PSM with 0.12 µm/pixel resolution, z-stack is set to 0.27 µm and multipoints with 512×512 pixels are defined for XY. Tile sizes are 60 × 60 µm. NIS-Elements software was used to stitch all tiles of the PSM with 5% overlap, which was imaged using XY multipoints.

Quantify single cell RNA numbers

The PSM was cleaned on z-slices and then masked by using membrane and nucleus signal with the Imaris surface tool[36]. Then, segmenting single cells on PSM tissue was done by using the Imaris 10 Cell module. For RNA number counting in each cell, spot detection was used with a diameter of 0.5 µm, background subtraction was enabled, and a "Quality" score was used to pick up true RNA signal. Background RNA numbers of *her1* and *her7* were calculated from the somite region[36] while those of *deltaC* and *deltaD* were calculated from notochord (because *deltaC* and *deltaD* are also expressed in somites). Distribution of RNA numbers do not show any bimodality (Figs. 1m–o, 3f–h, 4c, 5c, h and Supplementary Fig. 3), suggesting cell-to-cell heterogeneity is not abnormally high.

Single cell segmented PSM tissue data were collected for each sample in Excel. According to these analyses, further graphs were plotted on GraphPad to compare *her1* and *her7* RNAs in different genotypes.

Identification of potential NICD binding sites in the genomic regions nearby of *deltaC* and *deltaD* genes

The NICD protein binds to DNA through the RBPJ protein, which recognizes the consensus sequence TGGGAA. To identify potential NICD binding sites near the *deltaC* and *deltaD* genes, we conducted a search for RBPJ binding sites. Motif scanning was performed in the genomic regions surrounding the *deltaC* and *deltaD* genes in Danio rerio (zebrafish), extending 10 kb upstream and downstream of their loci on chromosome 13 (GRCz11 assembly). The PWMScan tool (https://epd.expasy.org/pwmtools)[37] was used for the analysis, applying the position-specific weight matrix (PWM) for the RBPJ motif (MA1116.2) from the JASPAR 2020 database[38]. Predicted binding sites were filtered based on PWM scores and P-values to ensure high-confidence results, reflecting binding strength and statistical significance. Each site was annotated with genomic coordinates, sequences, and strand orientation for further analysis.

Computational model

Mass action kinetics describes the interaction between reactants and products in chemical reactions, where the reaction rate is directly proportional to the concentration of the reactants. We have employed mass action kinetics to formulate our model for two cells. We updated our previously published time-delay differential equation models[21,33]. To account for the differential roles of different Delta protein dimers in transcription, we incorporated the transcriptional efficiency of each dimer[39]. Our current model consists of 23 equations and 65 parameters. Each equation describes the rate of change of mRNA, monomer protein, or dimer protein levels. The deterministic model was solved numerically using Euler's Method[40]. By increasing the time in specified step size, Euler's Method updates mRNA and protein levels in each iteration based on the rate of changes determined by the model.

We conducted pseudo-stochastic simulations of our model to incorporate the inherent randomness of biochemical reactions, as in our previous study[33]. This approach allowed each cell to exhibit up to 10% variation in biochemical reaction rates. Randomly selected parameter values from a biologically relevant range were perturbed by up to ±5% for each cell. This approach reflects the stochastic nature of the biochemical process and provides a more realistic simulation of the dynamics of this network. The parameter ranges and a sample parameter set used for the model simulations in Fig. 6a–c are shown in Table S2.

Model details

The equations governing molecule concentrations in simulations are as follows:

$$mdC_{den} = 1 + \left(\frac{ph1,1(t-\tau_{mdC})}{critph1,1}\right)^2 + \left(\frac{ph6,7(t-\tau_{mdC})}{critph6,7}\right)^2 + \left(\frac{pdC,C_n(t-\tau_{mdC})}{critpdC,C}\right) + \left(\frac{pdC,D_n(t-\tau_{mdC})}{critpdC,D}\right) + \left(\frac{pdD,D_n(t-\tau_{mdC})}{critpdD,D}\right)$$

$$\frac{d(mdC)}{dt} = \max K^{syn}_{mdC} \times \left(\frac{1}{mdC_{den}} \times E_1 + \frac{pdC,C_n(t-\tau_{mdC})}{critpdC,C \times mdC_{den}} \times E_{CC} + \frac{pdC,D_n(t-\tau_{mdC})}{critpdC,D \times mdC_{den}} \times E_{CD} + \frac{pdD,D_n(t-\tau_{mdC})}{critpdD,D \times mdC_{den}} \times E_{DD}\right) - K^{\deg}_{mdC} \times mdC$$

$$mdD_{den} = 1 + \left(\frac{pdC,C_n(t-\tau_{mdD})}{critpdC,C}\right) + \left(\frac{pdC,D_n(t-\tau_{mdD})}{critpdC,D}\right) + \left(\frac{pdD,D_n(t-\tau_{mdD})}{critpdD,D}\right)$$

$$\frac{d(mdD)}{dt} = \max K_{mdD}^{syn} \times \left(\frac{1}{mdD_{den}} \times E_1 + \frac{pdC, C_n(t-\tau_{mdD})}{critpdC, C \times mdD_{den}} \times E_{CC} + \frac{pdC, D_n(t-\tau_{mdD})}{critpdC, D \times mdD_{den}} \times E_{CD} + \frac{pdD, D_n(t-\tau_{mdD})}{critpdD, D \times mdD_{den}} \times E_{DD}\right) - K_{mdD}^{\deg} \times mdD$$

$$\frac{d(pdC)}{dt} = K_{pdC}^{syn} \times mdC\left(t-\tau_{pdC}\right) - K_{pdC}^{\deg} \times pdC + 2 \times K_{pdC,C}^{d} \times pdC, C + K_{pdC,D}^{d} \times pdC, D - 2 \times K_{pdC,C}^{a} \times pdC \times pdC - K_{pdC,D}^{a} \times pdC \times pdD$$

$$\frac{d(pdD)}{dt} = K_{pdD}^{syn} \times mdD\left(t-\tau_{pdD}\right) - K_{pdD}^{\deg} \times pdD + 2 \times K_{pdD,D}^{d} \times pdD, D + K_{pdC,D}^{d} \times pdC, D - 2 \times K_{pdD,D}^{a} \times pdD \times pdD - K_{pdC,D}^{a} \times pdC \times pdD$$

$$\frac{d(pdC, C)}{dt} = K_{pdC,C}^{a} \times pdC \times pdC - K_{pdC,C}^{d} \times pdC, C - K_{pdC,C}^{\deg} \times pdC, C$$

$$\frac{d(pdC, D)}{dt} = K_{pdC,D}^{a} \times pdC \times pdD - K_{pdC,D}^{d} \times pdC, D - K_{pdC,D}^{\deg} \times pdC, D$$

$$\frac{d(pdD, D)}{dt} = K_{pdD,D}^{a} \times pdD \times pdD - K_{pdD,D}^{d} \times pdD, D - K_{pdD,D}^{\deg} \times pdD, D$$

$$mh1_{den} = 1 + \left(\frac{ph1, 1(t-\tau_{mh1})}{critph1, 1}\right)^2 + \left(\frac{ph6, 7(t-\tau_{mh1})}{critph6, 7}\right)^2 + \left(\frac{pdC, C_n(t-\tau_{mh1})}{critpdC, C}\right) + \left(\frac{pdC, D_n(t-\tau_{mh1})}{critpdC, D}\right) + \left(\frac{pdD, D_n(t-\tau_{mh1})}{critpdD, D}\right)$$

$$\frac{d(mh1)}{dt} = \max K_{mh1}^{syn} \times \left(\frac{1}{mh1_{den}} \times E_1 + \frac{pdC, C_n(t-\tau_{mh1})}{critpdC, C \times mh1_{den}} \times E_{CC} + \frac{pdC, D_n(t-\tau_{mh1})}{critpdC, D \times mh1_{den}} \times E_{CD} + \frac{pdD, D_n(t-\tau_{mh1})}{critpdD, D \times mh1_{den}} \times E_{DD}\right) - K_{mh1}^{\deg} \times mh1$$

$$\frac{d(ph1)}{dt} = K_{ph1}^{syn} \times mh1\left(t-\tau_{ph1}\right) - K_{ph1}^{\deg} \times ph1 + 2 \times K_{ph1,1}^{d} \times ph1, 1 + K_{ph1,7}^{d} \times ph1, 7 + K_{ph1,6}^{d} \times ph1, 6 - ph1 \times \left(2 \times K_{ph1,1}^{a} \times ph1 + K_{ph1,7}^{a} \times ph7 + K_{ph1,6}^{a} \times ph6\right)$$

$$mh7_{den} = 1 + \left(\frac{ph1, 1(t-\tau_{mh7})}{critph1, 1}\right)^2 + \left(\frac{ph6, 7(t-\tau_{mh7})}{critph6, 7}\right)^2 + \left(\frac{pdC, C_n(t-\tau_{mh7})}{critpdC, C}\right) + \left(\frac{pdC, D_n(t-\tau_{mh7})}{critpdC, D}\right) + \left(\frac{pdD, D_n(t-\tau_{mh7})}{critpdD, D}\right)$$

$$\frac{d(mh7)}{dt} = \max K_{mh7}^{syn} \times \left(\frac{1}{mh7_{den}} \times E_1 + \frac{pdC, C_n(t-\tau_{mh7})}{critpdC, C \times mh7_{den}} \times E_{CC} + \frac{pdC, D_n(t-\tau_{mh7})}{critpdC, D \times mh7_{den}} \times E_{CD} + \frac{pdD, D_n(t-\tau_{mh7})}{critpdD, D \times mh7_{den}} \times E_{DD}\right) - K_{mh7}^{\deg} \times mh7$$

$$\frac{d(ph7)}{dt} = K_{ph7}^{syn} \times mh7\left(t-\tau_{ph7}\right) - K_{ph7}^{\deg} \times ph7 + 2 \times K_{ph7,7}^{d} \times ph7, 7 + K_{ph1,7}^{d} \times ph1, 7 + K_{ph6,7}^{d} \times ph6, 7 - ph7 \times \left(2 \times K_{ph7,7}^{a} \times ph7 + K_{ph1,7}^{a} \times ph1 + K_{ph6,7}^{a} \times ph6\right)$$

$$\frac{d(mh6)}{dt} = K_{mh6}^{syn} - K_{mh6}^{\deg} \times mh6$$

$$\frac{d(ph6)}{dt} = K_{ph6}^{syn} \times mh6\left(t-\tau_{ph6}\right) - K_{ph6}^{\deg} \times ph6 + 2 \times K_{ph6,6}^{d} \times ph6, 6 + K_{ph1,6}^{d} \times ph1, 6 + K_{ph6,7}^{d} \times ph6, 7 - ph6 \times \left(2 \times K_{ph6,6}^{a} \times ph6 + K_{ph1,6}^{a} \times ph1 + K_{ph6,7}^{a} \times ph7\right)$$

$$\frac{d(ph1, 1)}{dt} = K_{ph1,1}^{a} \times ph1 \times ph1 - K_{ph1,1}^{d} \times ph1, 1 - K_{ph1,1}^{\deg} \times ph1, 1$$

$$\frac{d(ph7, 7)}{dt} = K_{ph7,7}^{a} \times ph7 \times ph7 - K_{ph7,7}^{d} \times ph7, 7 - K_{ph7,7}^{\deg} \times ph7, 7$$

$$\frac{d(ph6, 6)}{dt} = K_{ph6,6}^{a} \times ph6 \times ph6 - K_{ph6,6}^{d} \times ph6, 6 - K_{ph6,6}^{\deg} \times ph6, 6$$

$$\frac{d(ph1, 7)}{dt} = K_{ph1,7}^{a} \times ph1 \times ph7 - K_{ph1,7}^{d} \times ph1, 7 - K_{ph1,7}^{\deg} \times ph1, 7$$

$$\frac{d(ph1, 6)}{dt} = K_{ph1,6}^{a} \times ph1 \times ph6 - K_{ph1,6}^{d} \times ph1, 6 - K_{ph1,6}^{\deg} \times ph1, 6$$

$$\frac{d(ph6, 7)}{dt} = K_{ph6,7}^{a} \times ph6 \times ph7 - K_{ph6,7}^{d} \times ph6, 7 - K_{ph6,7}^{\deg} \times ph6, 7$$

The transcriptional processes for *deltaC* and *deltaD* mRNAs, denoted as *mdC* and *mdD* respectively, are governed by specific synthesis and degradation rates. These rates are represented as $\max K_{mdC}^{syn}$ and $K_{mdC}^{\deg}$ for *deltaC* mRNA synthesis and degradation, and $\max K_{mdD}^{syn}$ and K_{mdD}^{syn} for *deltaD* mRNA synthesis and degradation. The corresponding DeltaC and DeltaD proteins, denoted as *pdC* and *pdD*, are synthesized and degraded at rates K_{pdC}^{syn}, $K_{pdC}^{\deg}$, K_{pdD}^{syn}, and $K_{pdD}^{\deg}$. DeltaC and DeltaD proteins form dimers and are denoted as follows: *pdC,C* for DeltaC/DeltaC, *pdC,D* for DeltaC/DeltaD, and *pdD,D* for DeltaD/DeltaD, with their respective degradation rates $K_{pdC,C}^{\deg}$, $K_{pdC,D}^{\deg}$, and $K_{pdD,D}^{\deg}$.

For *her1*, *her7*, and *hes6* mRNAs, represented as *mh1*, *mh7*, and *mh6*, the synthesis and degradation rates are $\max K_{mh1}^{syn}$, $K_{mh1}^{\deg}$, $\max K_{mh7}^{syn}$, $K_{mh7}^{\deg}$, and K_{mh6}^{syn}, $K_{mh6}^{\deg}$ respectively. The corresponding proteins Her1, Her7, and Hes6, denoted as *ph1*, *ph7*, and *ph6*, have synthesis and degradation rates K_{ph1}^{syn}, $K_{ph1}^{\deg}$, K_{ph7}^{syn}, $K_{ph7}^{\deg}$, and K_{ph6}^{syn}, $K_{ph6}^{\deg}$. Her1, Her7 and Hes6 protein dimers are represented as *ph1,1* (Her1-Her1), *ph7,7* (Her7-Her7), *ph6,6* (Hes6-Hes6), *ph1,7* (Her1-Her7), *ph1,6* (Her1-Hes6), and *ph6,7* (Hes6-Her7), with their respective degradation rates

$$K_{ph1,1}^{\deg}, K_{ph7,7}^{\deg}, K_{ph6,6}^{\deg}, K_{ph1,7}^{\deg}, K_{ph1,6}^{\deg}, \text{and} K_{ph6,7}^{\deg}$$

The binding and unbinding of protein dimers are characterized by their association and dissociation rates. The DeltaC/DeltaC, DeltaC/DeltaD, and DeltaD/DeltaD dimers have association and dissociation rates denoted by $K_{pdC,C}^{a}$ and $K_{pdC,C}^{d}$, $K_{pdC,D}^{a}$ and $K_{pdC,D}^{d}$, and $K_{pdD,D}^{a}$ and $K_{pdD,D}^{d}$, respectively. Similarly, for $i, j \in \{1, 6, 7\}$ where $i \leq j$, dimer protein *phi,j* has an association rate $K_{phi,j}^{a}$ and dissociation rate $K_{phi,j}^{d}$.

In this model, the transcription of *deltaC*, *her1*, and *her7* mRNA is repressed by Her1-Her1 and Her7-Hes6 dimers within the cell. The transcriptional activation driven by Delta-Notch signaling is provided in the transcription terms for *deltaC*, *deltaD, her1*, and *her7* mRNAs. The impact of DeltaC and DeltaD proteins on mRNA synthesis in the neighboring cell, facilitated by their interaction with the Notch receptor, is determined by evaluating the levels of DeltaC/DeltaC, DeltaC/DeltaD, and DeltaD/DeltaD dimers from neighboring cells (denoted with a subscript n in the equations to represent their values in adjacent cells). The Her and Delta protein dimer concentration levels have been used to calculate the probability of each promoter state. To calculate the final transcription term for each mRNA, the probability of each promoter state is multiplied by the efficiency of each activation state, denoted as E_1, E_{CC}, E_{CD} and E_{DD} in the equations, as described previously[39].

Parameter search

Due to technical difficulties, most reaction rates in zebrafish segmentation clock networks have not been precisely measured experimentally. We, therefore, utilized the Genetic Algorithm (GA) toolbox in MATLAB to perform a parameter search, which involves simulating a population of possible parameter sets and evolving these sets over generations[41]. At each step, the GA selects parameter sets that better reproduce the experimental observations of zebrafish segmentation clocks, using a fitness function designed to minimize the deviation between the model's predictions and empirical data. The initial parameter set consisted of randomly generated parameter values within a biologically relevant range, and pseudo-stochastic simulations were then performed using the generated parameters. This evolutionary process continues until it converges on a set of parameters that most closely align with the observed biological phenomena. From the refined parameters, we selected 11 sets that best fit the experimental observations to generate the model result figures (Fig. 6d, e). Similarly, to investigate the role of positive feedback, we simulated our model with and without positive feedback loop to achieve sustained oscillations with a 30 min period. We then recorded the synchrony score for 50 parameter sets for each model (Fig. 6f).

Oscillation features

In analyzing oscillatory behavior in dynamic systems, sustained oscillation characteristics are assessed using the final three-quarters of the simulation data to minimize the influence of initial transient effects. The oscillation amplitude is calculated at the midpoint's nearest peak-to-trough, and the ratio of peaks to troughs is checked at both the midpoint and the end to ensure that oscillations are sustained throughout the simulations. The period of oscillations is determined by identifying the time points of consecutive peaks within the simulation, excluding the first two peaks to mitigate initial transient effects. Synchronization disruption between two oscillating cells is determined using a synchronization score threshold of 0.8. This score, derived from the correlation over consecutive peak-to-trough phases, pinpoints the time index where the score first falls below the threshold, marking the point of synchronization disruption. These conditions have been checked using the core clock gene *her1* mRNA levels.

Coding

The codes for computational simulations have been implemented in MATLAB and tested with MATLAB R2024a. Image analysis is performed by using MATLAB and Python software then tested with MATLAB R2024b and Python (version 3.7)[36].

Reporting summary

Further information on research design is available in the Nature Portfolio Reporting Summary linked to this article.

Data availability

The microscopy images generated in this study are deposited in the BioStudies database under accession code S-BSST1519; https://doi.org/10.6019/S-BSST1519. There will be no restrictions on data availability. Source data are provided with this paper.

Code availability

Custom Matlab codes are available at GitHub (https://github.com/ozbudak/Notch-Alpay-2024), which is archived in Zenodo with the identifier (https://doi.org/10.5281/zenodo.14873344).

References

1. Kovall, R. A., Gebelein, B., Sprinzak, D. & Kopan, R. The Canonical notch signaling pathway: structural and biochemical insights into shape, sugar, and force. *Dev. Cell* **41**, 228–241 (2017).
2. McDaniel, C., Simsek, M. F., Chandel, A. S. & Ozbudak, E. M. Spatiotemporal control of pattern formation during somitogenesis. *Sci. Adv.* **10**, eadk8937 (2024).
3. Miao, Y. & Pourquie, O. Cellular and molecular control of vertebrate somitogenesis. *Nat. Rev. Mol. Cell Biol.* **25**, 517–533 (2024).
4. Turnpenny, P. D. et al. Abnormal vertebral segmentation and the notch signaling pathway in man. *Dev. Dyn.* **236**, 1456–1474 (2007).
5. Mara, A., Schroeder, J., Chalouni, C. & Holley, S. A. Priming, initiation and synchronization of the segmentation clock by deltaD and deltaC. *Nat. Cell Biol.* **9**, 523–530 (2007).
6. Keskin, S. et al. Noise in the vertebrate segmentation clock is boosted by time delays but tamed by notch signaling. *Cell Rep.* **23**, 2175–2185 e2174 (2018).
7. van Eeden, F. J. et al. Mutations affecting somite formation and patterning in the zebrafish, Danio rerio. *Development* **123**, 153–164 (1996).
8. Julich, D. et al. beamter/deltaC and the role of Notch ligands in the zebrafish somite segmentation, hindbrain neurogenesis and hypochord differentiation. *Dev. Biol.* **286**, 391–404 (2005).
9. Holley, S. A., Geisler, R. & Nusslein-Volhard, C. Control of her1 expression during zebrafish somitogenesis by a delta-dependent oscillator and an independent wave-front activity. *Genes Dev.* **14**, 1678–1690 (2000).
10. Jiang, Y. J. et al. Notch signalling and the synchronization of the somite segmentation clock. *Nature* **408**, 475–479 (2000).
11. Riedel-Kruse, I. H., Muller, C. & Oates, A. C. Synchrony dynamics during initiation, failure, and rescue of the segmentation clock. *Science* **317**, 1911–1915 (2007).
12. Ozbudak, E. M. & Lewis, J. Notch signalling synchronizes the zebrafish segmentation clock but is not needed to create somite boundaries. *PLoS Genet.* **4**, e15 (2008).
13. Delaune, E. A., Francois, P., Shih, N. P. & Amacher, S. L. Single-cell-resolution imaging of the impact of notch signaling and mitosis on segmentation clock dynamics. *Dev. Cell* **23**, 995–1005 (2012).
14. Niwa, Y. et al. Different types of oscillations in Notch and Fgf signaling regulate the spatiotemporal periodicity of somitogenesis. *Genes Dev.* **25**, 1115–1120 (2011).
15. Yoshioka-Kobayashi, K. et al. Coupling delay controls synchronized oscillation in the segmentation clock. *Nature* **580**, 119–123 (2020).
16. Lewis, J. Autoinhibition with transcriptional delay: a simple mechanism for the zebrafish somitogenesis oscillator. *Curr. Biol.* **13**, 1398–1408 (2003).
17. Ferjentsik, Z. et al. Notch is a critical component of the mouse somitogenesis oscillator and is essential for the formation of the somites. *PLoS Genet.* **5**, e1000662 (2009).
18. Hubaud, A., Regev, I., Mahadevan, L. & Pourquie, O. Excitable dynamics and yap-dependent mechanical cues drive the segmentation clock. *Cell* **171**, 668–682 e611 (2017).
19. Zinani, O. Q. H., Keseroglu, K., Ay, A. & Ozbudak, E. M. Pairing of segmentation clock genes drives robust pattern formation. *Nature* **589**, 431–436 (2021).

20. Wright, G. J. et al. DeltaC and DeltaD interact as Notch ligands in the zebrafish segmentation clock. *Development* **138**, 2947–2956 (2011).
21. Ay, A., Knierer, S., Sperlea, A., Holland, J. & Özbudak, E. M. Short-lived her proteins drive robust synchronized oscillations in the zebrafish segmentation clock. *Development* **140**, 3244–3253 (2013).
22. Simsek, M. F. et al. Periodic inhibition of Erk activity drives sequential somite segmentation. *Nature* **613**, 153–159 (2023).
23. Keskin, S. et al. Regulatory network of the scoliosis-associated genes establishes rostrocaudal patterning of somites in zebrafish. *iScience* **12**, 247–259 (2019).
24. Giudicelli, F., Ozbudak, E. M., Wright, G. J. & Lewis, J. Setting the tempo in development: an investigation of the zebrafish somite clock mechanism. *PLoS Biol.* **5**, e150 (2007).
25. Simsek, M. F. & Ozbudak, E. M. Spatial Fold Change of FGF Signaling Encodes Positional Information for Segmental Determination in Zebrafish. *Cell Rep.* **24**, 66–78 e68 (2018).
26. Zinani, O. Q. H. et al. Gene copy number and negative feedback differentially regulate transcriptional variability of segmentation clock genes. *iScience* **25**, 104579 (2022).
27. Zecchin, E., Conigliaro, A., Tiso, N., Argenton, F. & Bortolussi, M. Expression analysis of jagged genes in zebrafish embryos. *Dev. Dyn.* **233**, 638–645 (2005).
28. Prince, V. E. et al. Zebrafish lunatic fringe demarcates segmental boundaries. *Mech. Dev.* **105**, 175–180 (2001).
29. Dale, J. K. et al. Periodic Notch inhibition by Lunatic Fringe underlies the chick segmentation clock. *Nature* **421**, 275–278 (2003).
30. Okubo, Y. et al. Lfng regulates the synchronized oscillation of the mouse segmentation clock via trans-repression of Notch signalling. *Nat. Commun.* **3**, 1141 (2012).
31. Bochter, M. S. et al. Lfng and Dll3 cooperate to modulate protein interactions in cis and coordinate oscillatory Notch pathway activation in the segmentation clock. *Dev. Biol.* **487**, 42–56 (2022).
32. Holley, S. A. The genetics and embryology of zebrafish metamerism. *Dev. Dyn.* **236**, 1422–1449 (2007).
33. Ay, A. et al. Spatial gradients of protein-level time delays set the pace of the traveling segmentation clock waves. *Development* **141**, 4158–4167 (2014).
34. Tsai, T. Y. C. et al. Robust, tunable biological oscillations from interlinked positive and negative feedback loops. *Science* **321**, 126–129 (2008).
35. Bone, R. A. et al. Spatiotemporal oscillations of Notch1, Dll1 and NICD are coordinated across the mouse PSM. *Development* **141**, 4806–4816 (2014).
36. Keseroglu, K., Zinani, O. Q. H. & Ozbudak, E. M. Using single-molecule fluorescence in situ hybridization and immunohistochemistry to count RNA molecules in single cells in zebrafish embryos. *STAR Protoc.* **4**, 102020 (2023).
37. Ambrosini, G., Groux, R. & Bucher, P. PWMScan: a fast tool for scanning entire genomes with a position-specific weight matrix. *Bioinformatics* **34**, 2483–2484 (2018).
38. Fornes, O. et al. JASPAR 2020: update of the open-access database of transcription factor binding profiles. *Nucleic Acids Res.* **48**, D87–D92 (2020).
39. Dresch, J. M., Richards, M. & Ay, A. A primer on thermodynamic-based models for deciphering transcriptional regulatory logic. *Biochim. Biophys. Acta* **1829**, 946–953 (2013).
40. Sauer, T. *Numerical analysis*. Third edition. edn, (Pearson, 2018).
41. Sivanandam, S. N. & Deepa, S. N. *Introduction to genetic algorithms*. (Springer, 2007).

Acknowledgements

We thank Kemal Keseroglu, Didar Saparov, Abdullah Can Alpay, Matthew Kofron, Cincinnati Children's Imaging Core, Northwestern Feinberg Imaging Core, and Cincinnati Children's and Northwestern Feinberg Veterinary Services, and Colgate supercomputer (Partially funded by NSF Award #2346664) for technical assistance, and Fatma Rabia Urun-Bryant and Cassandra McDaniel for editing the text. This work was funded by an NIH grant (R35GM140805) to E.M.Ö.

Author contributions

E.M.Ö. and O.Q.H.Z. conceived the project. E.M.Ö. designed and supervised the project. E.E.A. performed experiments and analyzed the data. A.A. and X.H. wrote the computational code and run the simulations. E.M.Ö. wrote the manuscript. E.E.A., O.Q.H.Z., X.H., and A.A. edited the manuscript.

Competing interests

The authors declare no competing interests.

Additional information

Supplementary information The online version contains supplementary material available at https://doi.org/10.1038/s41467-025-57645-5.

Correspondence and requests for materials should be addressed to Ertuğrul M. Özbudak.

Peer review information *Nature Communications* thanks the anonymous reviewers for their contribution to the peer review of this work. A peer review file is available.